Revisiting the deuteron mass radius via near-threshold ρ^0, ω, and ϕ meson photoproduction*

Xiaoxuan Lin (林晓萱)[1,2] Wei Kou (寇维)[1,3] Shixin Fu (付士鑫)[1,3] Rong Wang (王荣)[1,3,4]
Chengdong Han (韩成栋)[1,3,4†] Xurong Chen (陈旭荣)[1,3,4,5‡]

[1]Institute of Modern Physics, Chinese Academy of Sciences, Lanzhou 730000, China
[2]College of Physics Science and Technology, Hebei University, Baoding 071002, China
[3]School of Nuclear Science and Technology, University of Chinese Academy of Sciences, Beijing 100049, China
[4]State Key Laboratory of Heavy Ion Science and Technology, Institute of Modern Physics, Chinese Academy of Sciences, Lanzhou 730000, China
[5]Southern Center for Nuclear Science Theory, Institute of Modern Physics, Chinese Academy of Sciences, Huizhou 516000, China

Abstract: We present a comprehensive analysis of near-threshold photoproduction of ρ^0, ω, and ϕ mesons on a deuterium target, utilizing published datasets from DESY and SLAC for ρ^0 and ω production, as well as data from the LEPS and CLAS Collaborations for ϕ production. In extracting the deuteron mass radius, we adopt a dipole parameterization for the scalar gravitational form factor, which effectively captures the $|t|$-dependence of the differential cross sections associated with vector meson photoproduction. In addition, results from alternative commonly used form factor parameterizations are considered and compared. By employing the vector meson dominance (VMD) framework and invoking low-energy Quantum Chromodynamics (QCD) theorems, we extract the deuteron mass radius from near-threshold photoproduction data of ρ^0, ω, and ϕ mesons. The mass radii obtained from the various datasets are found to be consistent within statistical uncertainties, yielding an average value of 2.03 ± 0.13 fm under the dipole form assumption. We also provide a detailed discussion of the sensitivity of the extracted radius to the choice of gravitational form factor models. Our result represents a significant improvement in precision compared to earlier estimates based solely on ϕ meson photoproduction, offering new constraints for theoretical models of nuclear structure and deepening our understanding of the mass distribution within the deuteron.

Keywords: mass radius, gravitational form factors, photoproduction

DOI: 10.1088/1674-1137/ade1c9 **CSTR:** 32044.14.ChinesePhysicsC.49103105

I. INTRODUCTION

The size of a proton, usually referred to as charge radius, magnetic radius, or mass radius, has always been a subject of contentious discussions. Due to the differences in proton charge radius observed in high-precision measurements, the study of proton radius has always been the focal point of theoretical and experimental research, which is often referred to as the proton charge radius puzzle [1−3]. The nucleon magnetic radius [4−6] is a fundamental parameter that characterizes the spatial distribution of nucleon magnetization, which originates from the motion and intrinsic magnetic moment of its constituent quarks and gluons. The mass radius of a nucleon describes the spatial distribution of mass within the nucleon, characterized by the mass density distribution. As a fundamental property of composite systems, the mass radius spans a vast range of scales, from subatomic particles in high-energy physics to galaxies in astrophysics. Recently, significant progress has been made in the determination and interpretation of nucleon and light-nuclei mass radii using various experimental and theoretical approaches [7−11]. The mass of a particle can be regarded as the response of the particle to the external gravitational field, and the gravitational form factor (GFF) of a particle is defined as the off-forward matrix element of the energy-momentum tensor (EMT) in the particle state [8, 12−15]. At low energy, the photoproduction of a quarkonium off the particle is connected to the scalar GFF of the particle, which is sensitive to the particle mass distribution from

Received 16 April 2025; Accepted 4 June 2025; Published online 5 June 2025

* Supported by the National Natural Science Foundation of China (12305127), the International Partnership Program of the Chinese Academy of Sciences (016GJHZ2022054FN), and National Key R&D Program of China (2024YFE0109800, 2024YFE0109802)

† E-mail: chdhan@impcas.ac.cn (Corresponding Author)
‡ E-mail: xchen@impcas.ac.cn (Corresponding Author)

the QCD trace anomaly.

Experimentally, the form factor $F(q)$ of the target is measured as a function of the momentum transfer q in the low momentum elastic scattering process and represents the Fourier transform of the density distributions $\rho(r)$, providing crucial insights into the internal structure of the nucleon, as described by QCD. The form factor enables researchers to access information about internal energy-momentum distributions inside the particle, thus directly linking experimental observables to fundamental QCD predictions [16]. For different hadronic systems, the internal density distributions are different, corresponding to different form factor parameterizations and root-mean-square radii of the particle. Specifically, this mass radius provides insights into the mass density distribution within nuclear systems, directly linked to underlying quark and gluon dynamics [17, 18]. The experimental determination of the proton and deuteron charge radii has also received renewed attention from facilities worldwide, including experiments using electron-proton and electron-deuteron scattering, muonic atoms spectroscopy, and vector meson photoproduction processes [19−21]. Similarly, understanding the deuteron mass radius, which describes the mass distribution within the deuteron, is essential for deepening our knowledge of the structure of the atomic nucleus. Notably, recent analyses of vector meson photoproduction near the production threshold have demonstrated their capability as sensitive probes for extracting nuclear mass distributions and radii. Currently, based on some vector meson near-threshold photoproduction data, several studies have aimed to extract the mass radii of nucleons and light-nuclei [7−11].

In this study, we systematically investigate the mass radius of the deuteron by analyzing the momentum transfer ($|t|$) dependence of differential cross sections from near-threshold photoproduction of the vector mesons ω, ρ^0, and ϕ. By combining careful experimental data analysis with rigorous theoretical modeling, we aim to provide reliable results contributing to the ongoing development of nuclear structure physics and QCD phenomenology. The organization of this paper is as follows. Section II briefly introduces the GFF and mass radius. Section III presents the data analysis and results. Finally, a short summary is given in Sec. IV.

II. GRAVITATIONAL FORM FACTOR AND MASS RADIUS

In a nonrelativistic and weak gravitational field approximation, the scalar GFF provides a useful framework for describing a particle mass distribution. That is, the mass radius of a particle can be theoretically defined in terms of the scalar GFF $G(t=q^2)$, the form factor of the trace of the QCD EMT instead of the form factor of T_{00} [8]. The GFF can be obtained via the measurement of generalized parton distributions (GPDs) from various exclusive scattering processes, as their second Mellin moments yield combinations of GFFs [14, 15]. In this study, a possible approach is to transform the study of graviton-nucleon scattering into the scalar GFF of the nucleon under the theoretical framework of the vector meson dominated (VMD) model. For a continuous mass density distribution at small momentum transfer $t=q^2$, the root-mean-square (RMS) radius of the nucleon is directly related to the slope of the scalar GFF at zero momentum transfer ($t=0$), expressed by [8, 22, 23]

$$\left\langle R_m^2 \right\rangle = 6\frac{\mathrm{d}G(t)}{\mathrm{d}t}\Big|_{t=0}, \tag{1}$$

where the scalar GFF is normalized to $G(0)=M$ at zero momentum transfer $t=0$.

For this analysis, the VMD model is used to describe near-threshold photoproduction processes of vector mesons on nuclear targets. The VMD model has been successfully applied in light vector meson near-threshold photoproductions studies [24−29], accurately linking measurable differential cross sections to the internal mass distributions of nucleons and light-nuclei [7−11, 30], as well as the vector-meson nucleon scattering lengths [24−29], among others. Specifically, at energies near the photoproduction threshold and at small momentum transfer ($|t| \ll 1\ \mathrm{GeV}^2$), the VMD model approximates the differential cross section by relating it directly to the square of the scalar GFF [8, 9]. Due to the near-nonrelativistic nature of heavy quarkonia produced in near-threshold photoproduction experiments, the coupling between the color-neutral heavy quark–antiquark pair and gluons can be described by the gluonic operator $g^2\mathbf{E}^{a2}$ [8]. This process is analogous to the Stark effect in QCD. The presence of this gluonic operator effectively encapsulates the interaction of the heavy quark pair with the gluon field in the nonrelativistic limit. Under these conditions, the near-threshold vector meson photoproduction amplitude can be factorized into a short-distance vacuum polarization contribution describing the photon splitting into a quark–antiquark pair and a nonperturbative matrix element of the gluonic operator $g^2\mathbf{E}^{a2}$ evaluated between the initial and final nuclear states [8]

$$\mathcal{M}_{\gamma N\to\psi N}(t) = -e_q c_2 2M\langle p_2|g^2\mathbf{E}^{a2}|p_1\rangle, \tag{2}$$

where $t=p_1-p_2$ is the momentum transfer, e_q is the charge of the quark, and c_2 is a coefficient representing the short-distance coupling between a heavy quark and the color electric field. It also includes the process of the quark pair transforming into a vector meson.

At this stage, the gluonic operator can be expressed in terms of the trace part of the EMT. When inserted into

the matrix element of the EMT, it yields a representation in terms of GFFs:

$$\mathcal{M}_{\gamma N\to\psi N}(t) = -e_q c_2 \frac{16\pi^2 M}{b_0}\langle p_2|T|p_1\rangle, \tag{3}$$

with

$$\langle p_1|T|p_2\rangle = \left(\frac{M_N^2}{p_{01}p_{02}}\right)^{1/2}\bar{u}(p_1,s_1)u(p_2,s_2)G(t) \sim G(t). \tag{4}$$

Therefore, the differential cross section for quarkonium near-threshold photoproduction processes in the small $-|t|$ region can be described with the scalar GFF as follows:

$$\frac{\mathrm{d}\sigma}{\mathrm{d}t} \propto G^2(t). \tag{5}$$

The validity of the above equation in describing the photoproduction of light vector mesons off the nucleon or hadronic matter is clear. Brodsky *et al*. [31] demonstrated that, in the small momentum transfer regime, the distinctive features of forward differential cross section for any possible vector meson leptoproduction can be reasonably factorized in perturbative QCD based on the $q\bar{q}$ wave function of the vector meson and the target gluon distribution.

The dipole form factor from the exponential distribution well describes the form factor of the nucleon within a wide kinematical range. To quantitatively describe the t-dependence of the experimental data and subsequently extract the deuteron mass radius, we adopt a widely-used dipole form parameterization for the scalar GFF [8, 9], written as

$$G(t) = \frac{M}{(1-t/\Lambda^2)^2}, \tag{6}$$

where Λ is a dipole parameter determined from fitting differential cross-section data. This simple and effective parameterization has demonstrated its ability to reliably reproduce experimental differential cross sections across multiple vector meson photoproduction channels [9]. More importantly, the dipole form factor has long been employed to describe double-gluon exchange processes in low-energy vector meson–nucleon scattering [32]. This underpins the rationale that, within the weak-gravity approximation, the exchange of two gluons —or a tensor glueball—can effectively serve as a surrogate for graviton–nucleon or graviton–nucleus scattering. While it is practically impossible to construct a direct graviton–nucleon scattering experiment, such processes are holographically dual to each other in the framework of holographic QCD [33−35]. Nevertheless, the current experimental precision is not sufficient to rule out alternative form factor models. In the following, we compare the commonly used parameterizations with the dipole ansatz.

III. DATA ANALYSIS AND RESULTS

Different hadronic systems exhibit distinct internal density distributions. Table 1 summarizes several representative density profiles, along with their corresponding form factors and mean square radii, assuming that $F(q) = G(q)/M$ is the normalized form factor. For mesons, such as the pion, the density decreases rapidly with increasing radial distance and is typically described by a Yukawa-type potential. The associated form factor of the pion exhibits a monopole behavior. In contrast, the dipole form factor, derived from an exponential density distribution, provides a good description of the proton form factor over a broad range of momentum transfer. For heavy nuclei, such as lead, the density distribution reflects the saturation property of nuclear matter and can be approximately modeled by a uniform or Fermi distribution. Accordingly, we introduce several different para-

Table 1. Analytical forms of density distributions $\rho(r)$, form factors $F(q)$, and corresponding root-mean-square (RMS) radii $\sqrt{\langle r^2\rangle}$ for different models.

Model	$\rho(r)$	$F(q)$	$\sqrt{\langle r^2\rangle}$
Yukawa-type	$\frac{\Lambda^2}{4\pi r}\mathrm{e}^{-\Lambda r}$	$\frac{1}{1+q^2/\Lambda^2}$	$\sqrt{\frac{6}{\Lambda^2}}$
Exponential	$\frac{\Lambda^3}{8\pi}r\mathrm{e}^{-\Lambda r}$	$\frac{1}{(1+q^2/\Lambda^2)^2}$	$\sqrt{\frac{12}{\Lambda^2}}$
Tripole	$\frac{\Lambda^4}{48\pi}r^2\mathrm{e}^{-\Lambda r}$	$\frac{1}{(1+q^2/\Lambda^2)^3}$	$\sqrt{\frac{18}{\Lambda^2}}$
Fourthpole	$\frac{\Lambda^5}{384\pi}r^3\mathrm{e}^{-\Lambda r}$	$\frac{1}{(1+q^2/\Lambda^2)^4}$	$\sqrt{\frac{24}{\Lambda^2}}$
Gaussian	$\left(\frac{\Lambda^2}{\pi}\right)^{3/2}\mathrm{e}^{-\Lambda^2 r^2}$	$\mathrm{e}^{-q^2/(4\Lambda^2)}$	$\sqrt{\frac{3}{2\Lambda^2}}$
Uniform	$\frac{3}{4\pi R^3}\theta(R-r)$	$\frac{3j_1(qR)}{qR}$	$\sqrt{\frac{3R^2}{5}}$

meterizations of GFFs to analyze the vector meson photoproduction data. Later in this section, we first present the results of various form factor models in describing the data from different experimental collaborations, along with the corresponding extractions of the mass radius. A comprehensive analysis of the deuteron mass radius obtained from different models is provided in the final subsection.

A. Photoproduction of ρ^0 on deuteron

The ABHHM collaboration [36] has investigated the photoproduction of the ρ^0 differential cross section in a deuterium bubble chamber experiment at DESY, with a bremsstrahlung beam at energies between 1 and 5 GeV. We analyzed near-threshold ρ^0 meson photoproduction differential cross-section data on the deuterium target at $E_\gamma = 1.8$-$2.5\,\text{GeV}$. Two different resonance reconstruction models were considered: Model (i) employs the standard Breit-Wigner resonance profile, while Model (ii) incorporates the interference effects from Drell-type one-pion exchange. Figure 1 shows the differential cross sections $\mathrm{d}\sigma/\mathrm{d}t$ of ρ^0 meson photonproductions as a function of $-t$. In addition to the black solid curve corresponding to the dipole GFFs, the colored curves represent different parameterizations of the GFFs. Evidently, in the low-$|t|$ region, the distinct shapes of these models —stemming from the lack of experimental constraints—highlight the criticality of data in this kinematic domain. Differential cross sections are independently fitted for each model to extract the corresponding deuteron mass radius, and the deuteron mass radii with different GFFs are extracted from ABHHM data. The extracted values of the parameter Λ of GFFs and deuteron radius $\sqrt{\langle R_m^2\rangle}$ are listed in Table 2. It is evident that different models yield distinct descriptions of the same dataset, leading to variations in the extracted deuteron mass radius. However, the differences in the corresponding reduced χ^2 values are not substantial. This indicates that, within the available kinematic range of the data, all considered GFF parameterizations provide a reasonably good description of the differential cross sections.

B. Photoproduction of ω on deuteron

Eisenberg *et al.* [37] measured the coherent photoproduction of ω in γd interaction at $E_\gamma = 4.3$ GeV. The experiment was conducted by exposing the SLAC 40-inch bubble chamber to a quasi-monochromatic e^+ annihilation photon beam with an energy of 4.3 GeV. Figure 2 shows the differential cross sections of the near-threshold ω photoprodution reaction $\gamma\mathrm{d} \to \omega\mathrm{d}$ at $E_\gamma = 4.3$ GeV. From the fits of the dipole GFF, ω photoproduction differential cross-section data imply that the deuteron mass radius is $2.04 \pm 0.47\,\text{fm}$. The solid black curve shows the fit of the dipole scalar GFF model, the colored curves represent those of the other models. To quantify the quality of fit, the values of the obtained parameter Λ and the extracted deuteron radii $\sqrt{\langle R_m^2\rangle}$ from the differential cross sections of ω photoproduction near the threshold are listed in Table 3. It can be observed that, in contrast to the case of ρ^0 meson production, the deuteron mass radii extracted from the ω production data do not exhibit significant variations across different GFF models. All extracted radii fall within the range of approximately 1 to 2 fm, and the corresponding reduced χ^2 values remain relatively small. This behavior can be attributed to the fact that the ω production data lie within a lower $|t|$ kinematic regime, which provides somewhat stronger constraints on the models.

C. Photoproduction of ϕ on deuteron

In a previous study [7], we analyzed the coherent ϕ-photoproduction differential cross sections on a deuterium target from the CLAS and LEPS collaborations [38−41], obtaining a deuteron mass radius of 1.95 ± 0.19 fm. This value is consistent with the values extracted from the current ρ^0 and ω meson analyses with-

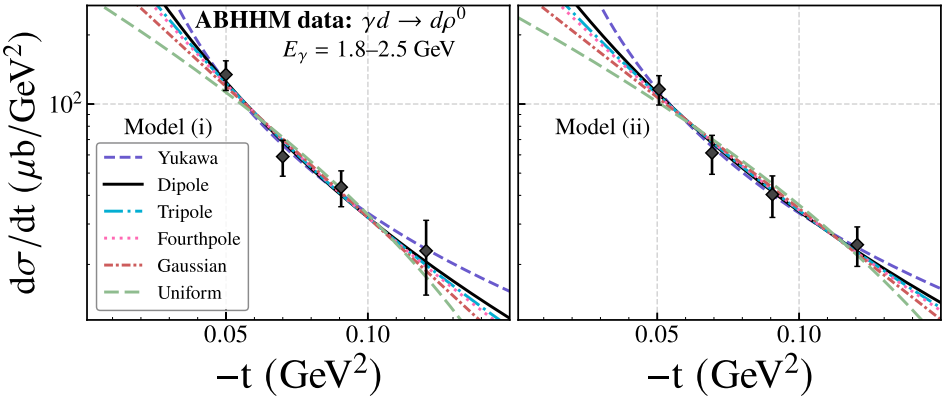

Fig. 1. (color online) Differential cross sections of near-threshold ρ^0 photoproduction on deuteron fitted with six models using two resonance schemes (Models (i) and (ii)) from ABHHM Collaboration data [36].

Table 2. Fitted results of Λ, deuteron mass radius $\sqrt{\langle R_m^2\rangle}$, and χ^2/ndf for different models from near-threshold ρ^0 photoproduction data measured by the ABHHM Collaboration [36]. Global averages are calculated by combining results from Models (i) and (ii).

ABHHM (Model (i))			
Model	Λ (GeV)	$\sqrt{\langle R_m^2\rangle}$ /fm	χ^2/ndf
Yukawa	0.06 ± 0.02	7.66 ± 2.25	0.85/2
Dipole	0.27 ± 0.05	2.52 ± 0.47	1.31/2
Tripole	0.38 ± 0.05	2.17 ± 0.32	1.55/2
Fourthpole	0.48 ± 0.06	2.04 ± 0.27	1.68/2
Gaussian	0.14 ± 0.01	1.75 ± 0.18	2.21/2
	R (GeV^{-1})		
Uniform	8.50 ± 0.63	1.30 ± 0.10	3.05/2
ABHHM (Model (ii))			
Model	Λ (GeV)	$\sqrt{\langle R_m^2\rangle}$ /fm	χ^2/ndf
Yukawa	0.10 ± 0.06	5.31 ± 3.85	0.16/2
Dipole	0.31 ± 0.05	2.23 ± 0.33	0.56/2
Tripole	0.42 ± 0.05	1.96 ± 0.23	0.75/2
Fourthpole	0.52 ± 0.06	1.85 ± 0.20	0.85/2
Gaussian	0.15 ± 0.01	1.61 ± 0.14	1.21/2
	R (GeV^{-1})		
Uniform	8.00 ± 0.50	1.22 ± 0.08	1.95/2
Global Average			
Model		$\sqrt{\langle R_m^2\rangle}$ /fm	
Yukawa		7.06 ± 1.95	
Dipole		2.33 ± 0.27	
Tripole		2.03 ± 0.18	
Fourthpole		1.92 ± 0.16	
Gaussian		1.66 ± 0.11	
Uniform		0.65 ± 0.01	

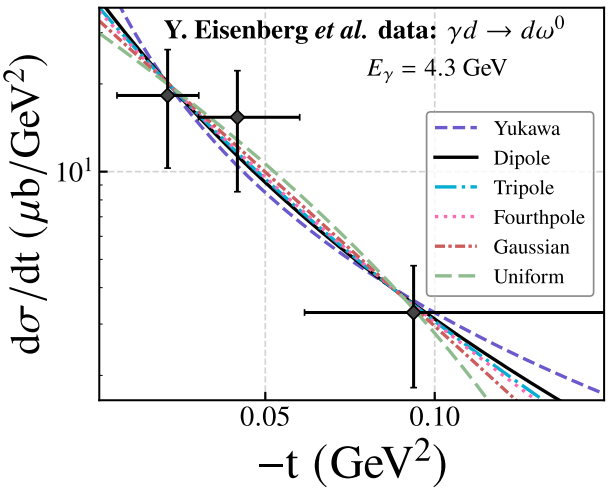

Fig. 2. (color online) Differential cross sections of near-threshold ω photoproduction measured by Eisenberg *et al.* [37], fitted with six models.

in statistical uncertainties, strongly supporting the robustness and universality of our theoretical approach across different vector meson channels.

To enable a more detailed comparison, we applied the various form factor models to the differential cross-section data of ϕ photoproduction reported by the CLAS and LEPS collaborations. The corresponding fit results are shown in Figs. 3 and 4, and the extracted model parameters, including the deuteron mass radius, are summarized in Table 4. It is worth emphasizing that the LEPS collaboration provides data under three photon energy configurations, all of which can be regarded as near-threshold. We find that the results obtained by independently fitting the data at each energy point and subsequently averaging are consistent with those derived from a global fit using the combined dataset across all energy configurations. In principle, the deuteron mass radius is a fundamental property and should be independent of the specific photon energy configuration used in the experiment. Therefore, as

Table 3. Fitted values of Λ, deuteron mass radius $\sqrt{\langle R_m^2 \rangle}$, and fit quality χ^2/ndf from the near-threshold ω photoproduction data measured by Eisenberg *et al.* [37].

Y. Eisenberg *et al.*			
Model	Λ /GeV	$\sqrt{\langle R_m^2 \rangle}$ /fm	χ^2/ndf
Yukawa	0.18 ± 0.07	2.68 ± 1.04	0.62/1
Dipole	0.33 ± 0.08	2.04 ± 0.47	0.43/1
Tripole	0.44 ± 0.09	1.90 ± 0.38	0.38/1
Fourthpole	0.52 ± 0.10	1.84 ± 0.35	0.35/1
Gaussian	0.14 ± 0.02	1.68 ± 0.27	0.28/1
	R (GeV^{-1})		
Uniform	8.76 ± 1.05	1.34 ± 0.16	0.19/1

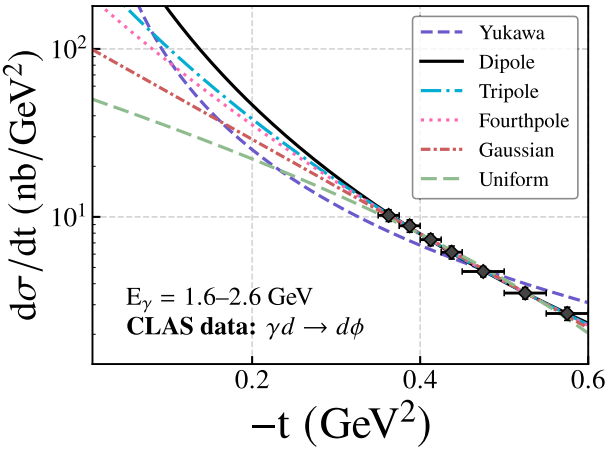

Fig. 3. (color online) Differential cross sections of near-threshold ϕ photoproduction measured by the CLAS Collaboration [39], fitted with six model parameterizations.

long as the condition of near-threshold production is satisfied, the extracted results are expected to be largely insensitive to the precise photon energy. In addition, the CLAS collaboration data are predominantly located in the region of $|t| > 0.3$ GeV^2, which leads to more pronounced variations in the fitted results.

D. Global analysis with ρ^0, ω, and ϕ photoproduction on deuteron

In summary, we have analyzed the near-threshold photoproduction data for all three types of vector mesons to extract the deuteron mass radius. The results, derived from different experimental collaborations, various vector meson probes, and distinct parameterizations of GFFs, consistently fall within the range of $1 \sim 2$ fm. With the exception of the Yukawa-type GFFs—which yield a mass radius larger than the known deuteron charge radius—all GFFs produce mass radii smaller than the charge radius [42, 43]. This indicates a strong possibility that the deuteron's energy density distribution is more compact than its charge distribution, although a certain degree of model dependence persists.

We used the following formula for the calculation of weightedaverage: $\bar{x} \pm \delta\bar{x} = \sum_i w_i x_i / \sum_i w_i \pm \left(\sum_i w_i\right)^{-1/2}$, with $w_i = 1/(\delta x_i)^2$. Note that the weighted average of the mass radii obtained here with different models is consistent with the result of the simultaneous fit to all the datasets. We performed a weighted average of the deuteron mass radii obtained from each individual parameterization of GFFs. The weighted average results from all six GFF parameterizations are presented in Fig. 5. The root-mean-square mass radii of deuteron are extracted from the fits described above, where each GFF model is used to describe the photoproduction data of ρ^0, ω, and ϕ mesons. In each panel, the horizontal line and its associated uncertainty band represent the weighted average of the three data points. The resulting mass radii from the weighted averages corresponding to the six GFF parameterizations are summarized in Table 5.

From the deuteron mass radii extracted using six commonly adopted distribution models, it is evident that the results associated with ρ^0 and ω meson photoproduction exhibit larger uncertainties compared to those from ϕ

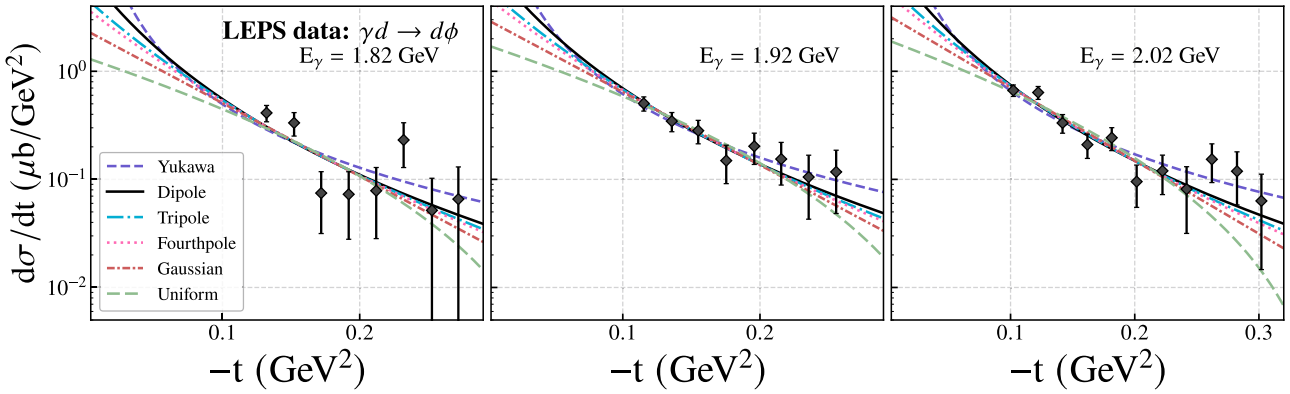

Fig. 4. (color online) Differential cross sections of near-threshold ϕ photoproduction measured by the LEPS Collaboration [41, 40], fitted with six model parameterizations.

Table 4. Fitted values of Λ, deuteron mass radius $\sqrt{\langle R_m^2\rangle}$, and fit quality χ^2/ndf obtained from near-threshold ϕ photoproduction data measured by the CLAS Collaboration [39] and LEPS Collaboration [40, 41].

CLAS			
Model	Λ /GeV	$\sqrt{\langle R_m^2\rangle}$ /fm	χ^2/ndf
Yukawa	0.12 ± 0.02	3.86 ± 0.76	25.66/5
Dipole	0.40 ± 0.05	1.71 ± 0.23	0.20/5
Fourthpole	0.88 ± 0.05	1.10 ± 0.06	0.23/5
Tripole	0.68 ± 0.05	1.22 ± 0.08	0.19/5
Gaussian	0.28 ± 0.01	0.87 ± 0.03	0.53/5
	R (GeV^{-1})		
Uniform	3.99 ± 0.08	0.61 ± 0.01	1.93/5
LEPS			
Model	Λ /GeV	$\sqrt{\langle R_m^2\rangle}$ /fm	χ^2/ndf
Yukawa	0.06 ± 0.01	8.26 ± 1.45	27.85/23
Dipole	0.32 ± 0.04	2.14 ± 0.26	24.01/23
Tripole	0.48 ± 0.04	1.75 ± 0.15	24.56/23
Fourthpole	0.60 ± 0.04	1.62 ± 0.12	24.94/23
Gaussian	0.18 ± 0.01	1.35 ± 0.07	26.51/23
	R (GeV^{-1})		
Uniform	6.32 ± 0.24	0.97 ± 0.04	31.83/23
Global Average			
Model		$\sqrt{\langle R_m^2\rangle}$ /fm	
Yukawa		4.82 ± 0.68	
Dipole		1.90 ± 0.17	
Tripole		1.36 ± 0.07	
Fourthpole		1.21 ± 0.05	
Gaussian		0.94 ± 0.03	
Uniform		0.65 ± 0.01	

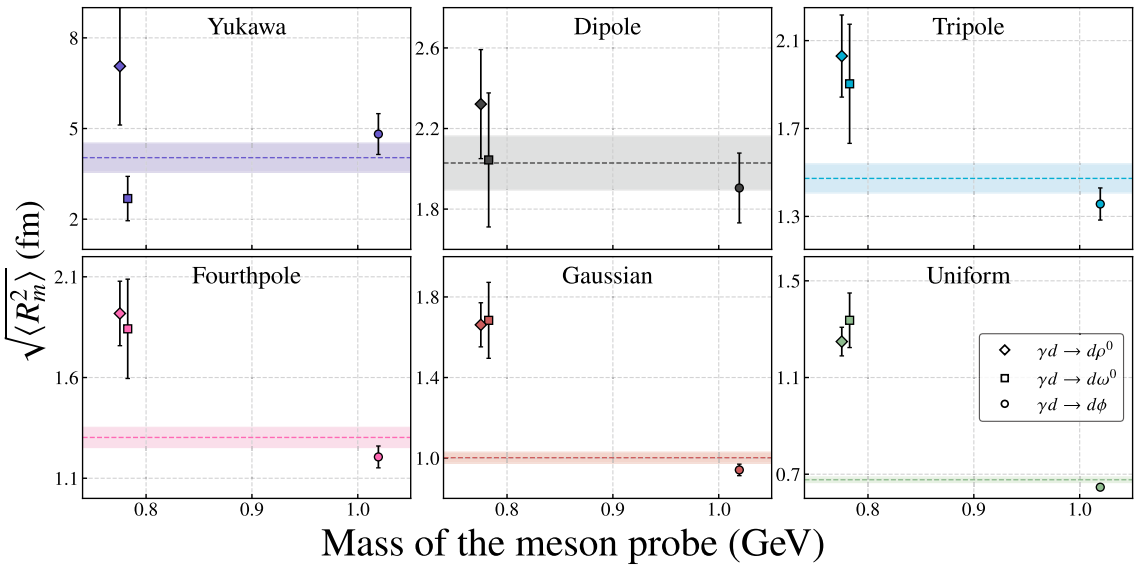

Fig. 5. (color online) Comparison of deuteron mass radii extracted with different parameterizations as a function of meson probe mass. Each subplot corresponds to a specific model.

Table 5. Final extracted deuteron mass radii $\sqrt{\langle R_m^2 \rangle}$ using different form factor models.

Model	$\sqrt{\langle R_m^2 \rangle}$ /fm
Yukawa	4.04 ± 0.48
Dipole	2.03 ± 0.13
Tripole	1.47 ± 0.07
Fourthpole	1.30 ± 0.05
Gaussian	1.00 ± 0.03
Uniform	0.68 ± 0.01

meson data. Consequently, the weighted average is more heavily influenced by the ϕ meson results. Moreover, the dipole-type GFFs yield more consistent radii across all three vector meson channels, indicating a stronger generalization capability in describing near-threshold photoproduction processes. This suggests that dipole-type GFFs are more robust in modeling the underlying dynamics. Future high-precision photoproduction experiments involving heavy vector mesons, such as J/ψ and Y, may provide additional constraints on GFFs. Based on these considerations, we favor extracting the deuteron mass radius within the framework of two-gluon exchange, as encapsulated by dipole-type GFFs. This approach has already demonstrated its advantages in previous determinations of proton and neutron mass radii.

IV. SUMMARY

Based on the assumptions of the VMD model and a low energy QCD theorem, we extracted the deuteron mass radius by systematically analyzing different vector meson near-threshold photoproduction data. By utilizing a dipole parameterization of the scalar GFF within the VMD framework, the combined analysis of the photoproduction of the three vector mesons ρ^0, ω, and ϕ off a deuteron gives the average radius to be 2.03 ± 0.13 fm (dipole GFFs), which is smaller than the world average of the deuteron charge radius (CODATA-2020 evaluation gives deuteron charge radius 2.1424 ± 0.0021 fm) [42, 43]. This result is in good agreement with the previous determination based solely on ϕ photoproduction near-threshold data [7], thereby reinforcing the validity and universality of the adopted approach. In fact, our ultimate goal is to determine the deuteron mass radius in a manner that is independent of both the incident photon energy and specific modeling choices. However, current experimental efforts toward extracting the mass radii of nucleons or nuclei still require extensive data accumulation and theoretical development. We argue that the deuteron mass radius, much like its charge radius, should be regarded as an intrinsic property that encodes information about the internal energy or mass distribution of the system. Nevertheless, our analysis indicates that different parameterizations of GFFs can yield notably distinct descriptions of the same set of differential cross-section data. This variation is primarily due to the limited number and precision of existing measurements, particularly the lack of data in the forward kinematic region, which significantly increases the uncertainties in the fits. Considering all factors, we conclude that the dipole-type GFFs constitute one of the most reliable choices—both in terms of physical interpretability and fit quality. However, more stringent model constraints will ultimately require high-precision measurements of forward differential cross sections.

This analysis provides not only necessary constraints for theoretical models of nuclear structure but also a deeper understanding of the spatial distribution of mass within the deuteron. The consistent deuteron mass extracted from different near-threshold vector meson photoproduction data indicates that the VMD model combined with the dipole parameterization of the scalar GFF is a powerful tool to probe the internal structure of deuteron. In addition, precisely extracting the mass radius of deuteron is crucial for understanding the interplay between quark-gluon dynamics and nuclear binding, as well as for refining our knowledge of generalized parton distributions, which are closely related to GFFs. Despite the success of our approach, several challenges remain. Currently, the approach to extracting the mass radius of deuterons parallels that of protons, meaning that the probe "sees" the structure of the entire nucleus without incorporating the shape of the deuteron itself into the size measurement process. Additionally, similar to the determination of proton mass radius, different vector meson probes yield nearly identical deuteron mass radii within the uncertainty ranges, indicating that the form factor may not be sensitive to the type of meson probe used. The relatively large uncertainties in some of the individual channels highlight the necessity of improving experimental precision, especially in the low momentum-transfer region. Future experimental campaigns at next-generation electron scattering facilities and near-threshold photoproduction experiments are expected to provide high precision data, which will enable further improvement of the extraction of deuteron mass radius and a more detailed mapping of the internal mass distribution.

In short, our comprehensive analysis in different vector meson photoproduction channels contributes to a deeper understanding of the deuteron structure and lays a solid foundation for future theoretical and experimental investigations in nuclear mass radius physics. The innovative extraction of the deuteron mass radius from various meson photoproduction processes highlights the prospect of combining advanced experimental techniques with rigorous theoretical modeling to reveal the complex structure of nuclear matter.

References

[1] R. Pohl *et al*., Nature **466**, 213 (2010)
[2] A. Antognini *et al*., Science **339**, 417 (2013)
[3] C. E. Carlson, Prog. Part. Nucl. Phys. **82**, 59 (2015)
[4] J. M. Alarcón, D. W. Higinbotham, and C. Weiss, Phys. Rev. C **102**, 035203 (2020), arXiv: 2002.05167[hep-ph]
[5] Y.-H. Lin, H.-W. Hammer, and U.-G. Meißner, Phys. Lett. B **816**, 136254 (2021), arXiv: 2102.11642[hep-ph]
[6] D. Djukanovic, G. von Hippel, H. B. Meyer *et al*., Phys. Rev. Lett. **132**, 211901 (2024), arXiv: 2309.07491[hep-lat]
[7] R. Wang, W. Kou, C. Han *et al*., Phys. Rev. D **104**, 074033 (2021), arXiv: 2108.03550[hep-ph]
[8] D. E. Kharzeev, Phys. Rev. D **104**, 054015 (2021)
[9] R. Wang, W. Kou, Y.-P. Xie *et al*., Phys. Rev. D **103**, L091501 (2021), arXiv: 2102.01610[hep-ph]
[10] C. Han, G. Xie, W. Kou *et al*., Eur. Phys. J. A **58**, 105 (2022), arXiv: 2201.08535[hep-ph]
[11] R. Wang, C. Han, and X. Chen, Phys. Rev. C **109**, L012201 (2024), arXiv: 2309.01416[hep-ph]
[12] I. Y. Kobzarev and L. B. Okun, Zh. Eksp. Teor. Fiz. **43**, 1904 (1962)
[13] H. Pagels, Phys. Rev. **144**, 1250 (1966)
[14] O. V. Teryaev, Front. Phys. (Beijing) **11**, 111207 (2016)
[15] M. V. Polyakov and P. Schweitzer, Int. J. Mod. Phys. A **33**, 1830025 (2018)
[16] X. Ji, Front. Phys. **16**, 64601 (2021)
[17] X. Ji, Phys. Rev. Lett. **78**, 610 (1997)
[18] V. D. Burkert, Nature **557**, 396 (2018)
[19] W. Xiong, Nature **575**, 147 (2019)
[20] H.-W. Hammer and U.-G. Meißner, Sci. Bull. **65**, 257 (2020)
[21] R. Dupré, M. Guidal, and M. Vanderhaeghen, Phys. Rev. D **103**, 014023 (2021)
[22] K. Kumerički, S. Liuti, and H. Moutarde, Eur. Phys. J. A **52**, 157 (2016)
[23] G. A. Miller, Phys. Rev. C **99**, 035202 (2019), arXiv: 1812.02714[nucl-th]
[24] I. I. Strakovsky *et al*., Phys. Rev. C **91**, 045207 (2015), arXiv: 1407.3465[nucl-ex]
[25] I. I. Strakovsky, L. Pentchev, and A. Titov, Phys. Rev. C **101**, 045201 (2020), arXiv: 2001.08851[hep-ph]
[26] L. Pentchev and I. I. Strakovsky, Eur. Phys. J. A **57**, 56 (2021), arXiv: 2009.04502[hep-ph]
[27] X.-Y. Wang, F. Zeng, and I. I. Strakovsky, Phys. Rev. C **106**, 015202 (2022), arXiv: 2205.07661[hep-ph]
[28] C. Han, W. Kou, R. Wang *et al*., Phys. Rev. C **107**, 015204 (2023), arXiv: 2210.11276[hep-ph]
[29] C. Han, W. Kou, R. Wang *et al*., Eur. Phys. J. A **59**, 118 (2023), arXiv: 2211.17102[hep-ph]
[30] W. Kou, R. Wang, and X. Chen, Phys. Rev. D **103**, 014025 (2021)
[31] S. J. Brodsky, L. Frankfurt, J. F. Gunion *et al*., Phys. Rev. D **50**, 3134 (1994), arXiv: hep-ph/9402283
[32] L. Frankfurt and M. Strikman, Phys. Rev. D **66**, 031502 (2002), arXiv: hep-ph/0205223
[33] K. A. Mamo and I. Zahed, Phys. Rev. D **101**, 086003 (2020), arXiv: 1910.04707[hep-ph]
[34] K. A. Mamo and I. Zahed, Phys. Rev. D **103**, 094010 (2021), arXiv: 2103.03186[hep-ph]
[35] K. A. Mamo and I. Zahed, Phys. Rev. D **106**, 086004 (2022), arXiv: 2204.08857[hepph]
[36] P. Benz, O. Braun, H. Butenschön *et al*., Nucl. Phys. B **79**, 10 (1974)
[37] Y. Eisenberg, B. Haber, E. Kogan *et al*., Nucl. Phys. B **38**, 349 (1972)
[38] H. Seraydaryan *et al*. (CLAS), Phys. Rev. C **89**, 055206 (2014), arXiv: 1308.1363[hep-ex]
[39] T. Mibe *et al*. (CLAS), Phys. Rev. C **76**, 052202(R) (2007), arXiv: nucl-ex/0703013
[40] T. Mibe *et al*. (LEPS), Phys. Rev. Lett. **95**, 182001 (2005), arXiv: nucl-ex/0506015
[41] W. C. Chang *et al*., Phys. Lett. B **658**, 209 (2008), arXiv: nucl-ex/0703034
[42] R. Pohl *et al*. (CREMA), Science **353**, 669 (2016)
[43] P. Mohr, D. Newell, B. Taylo *et al*., arXiv: 2409.03787 [hep-ph]